Drosophila larval gut transcriptome reveals a microbe-mediated intestinal tissue growth *via* Ecdysone during adaptive growth

Longwei Bai[1], Stéphanie Bellemin[2], Coralie Drelon[3], Pauline Joncour[4], Elodie Guillemot [5], Maura Strigini[6], Benjamin Gillet[1], François Leulier[1]* and Cathy Isaura Ramos[1]*

[1] Institut de Génomique Fonctionnelle de Lyon, Ecole Normale Supérieur de Lyon, Université Claude Bernard Lyon 1, CNRS UMR 5242, 46 allée d'Italie, 69007 Lyon
[2] Synbird, 14 Fbg Reclus, 73000 Chambéry
[3] CNRS UMR 7369 MEDyC - Reims University, Reims, France
[4] University of Rennes | UR1 · Ecosystèmes, Biodiversité, Evolution - UMR CNRS 6553 ECOBIO
5 Charles River Laboratories, 9 All. Moulin Berger, 69130 Écully
[6] University of Lyon, UJM Saint-Étienne, France - Faculty of Medicine and INSERM U1059-SAINBIOSE

*Co-corresponding authors
cathy.ramos@ens-lyon.fr, francois.leulier@ens-lyon.fr

Acknowledgements

The authors would like to thank Berra Erkosar for initial observations; Naoki Yamanaka for sharing reagents at the early stage of the project; Aurelio Teleman for his relevant comments; the Arthro-Tools platform of the UAR Biosciences (UMS3444/US8) for providing *Drosophila* facilities.

Competing interests

The authors declare no competing or financial interests.

Author contributions

Conceptualization: C.I.R. and F.L.; Methodology: C.I.R., C.D., S.B. and M.S.; Software: P.J; Validation: C.I.R., L.B and S.B.; Formal analysis: C.I.R.; Investigation: C.I.R. L.B. and E.G.; Resources: C.I.R., L.B., and B.G.; Data curation: C.I.R.; Writing - original draft: C.I.R.; Writing - review & editing: C.I.R. and F.L; Visualization: C.I.R.; Supervision: C.I.R. and F.L.; Project administration: C.I.R and F.L..; Funding acquisition: C.I.R. and F.L.

Funding

This project was supported by the "Fondation pour la Recherche Médicale" (« Equipe FRM DEQ20180339196), the Scientific Breakthrough Project from Université de Lyon "Microbehave" and an ERC starting grant (FP7/2007-2013-N°309704) to F.L. C.I.R was funded by the "UCBL" through a "Bonus Quality Recherche" scholarship and by FINOVI foundation for AO12-19-Projet SNI Ramos scholarship.

Keywords : organ growth, Ecdysone, *Drosophila* midgut, microbiota

Abstract

Juvenile growth is an adaptive trait since chronic undernutrition leads to reduced growth rate and delayed maturation. Using *Drosophila* and mouse gnotobiotic models, we previously established the evolutionarily conserved influence of the intestinal microbiota and selected *Lactobacilli* strains on juvenile growth. Here we aimed to identify the molecular mechanisms underlying microbe-mediated *Drosophila* adaptive growth. Since the intestine is the interface of host-microbe interactions, we conducted an analysis of the larval midgut transcriptome in presence or absence of an intestinal *Lactobacilli* strain representative of the *Drosophila* microbiota. Among the different biological processes identified, Ecdysone signaling has emerged as a new *Lactobacill*i-mediated signature. Through functional and morphometrical approaches, we show that, upon bacteria association, intestinal Ecdysone is not rate limiting for the larval systemic plastic growth but required for the adaptation of midgut growth to *Lactobacilli*. Our results reveal a tissue-specific contribution of the pleiotropic hormone Ecdysone in the control of midgut adaptive growth and maturation.

Introduction

In animals, organ growth is coupled with and coordinated to systemic growth. In addition, the organism adapts its growth to internal and external cues to allow the emergence of fit adults at the end of development. Nutrition is a prime cue influencing adaptive growth, the microbiota has also been shown to influence this important physiological function (Storelli et al. 2011) (Schwarzer et al. 2016).

In the malnourished *Drosophila* larvae, the mono-association of germ-free (GF) animals with *Lactiplantibacillus plantarum (Lp)*, a *Lactobacilli* representative member of the fly microbiota, can fully recapitulate the beneficial effects of an intact microbiota by supporting linear growth and maturation rates (Storelli et al. 2011). These effects involve a link between microbiome activities, enhanced host digestive capabilities and juvenile adaptive growth upon chronic undernutrition in *Drosophila* (Storelli et al. 2011) (Erkosar et al. 2015)(Matos et al. 2017)(Storelli et al. 2018). The systemic growth of *Drosophila* larvae is mainly modulated by two hormones: Insulins like-peptides (Ilps) and Ecdysone (Ecd). While Ilps directly regulate systemic growth rate (Colombani et al. 2003) (Géminard, Rulifson, and Léopold 2009), Ecd controls the growth period duration by regulating maturation through the different molts (Shingleton et al. 2005). Previously, we showed that in malnourished *Lp*-associated animals, systemic growth is supported by both Ecd and Ilps signals, under the control of TOR in the prothoracic gland and in the fat body, respectively (Storelli et al. 2011). Thus, microbiota members support growth through enhanced systemic activities of the two main hormones.

While the systemic and the cellular effects of Ilps are well studied, the precise understanding of the impact of Ecd in developing tissues remains incomplete owing to its confounding pleiotropic effects. Indeed, in *Drosophila* larva, Ecd signaling controls moltings at the systemic level and lead to either the growth, the remodeling or even the lysis of larval organs, while contributing to morphogenesis and differentiation of imaginal tissues (reviewed in (Boulan, Milán, and Léopold 2015). Ecd is synthetised from dietary cholesterol in the prothoracic gland (PG), under the control of the prothoracicotropic hormone (PTTH). Ecd is released from the PG in vesicles (Yamanaka, Marqués, and O'Connor 2015) and circulates to the peripheric tissues *via* haemolymph. The cellular uptake of Ecd relies on an active transport mediated by a family of transporters named Oatp (Organic anion transporting polypeptide) such as the Ecd Importer (EcI also called Oatp74D) in the larval fat body (Okamoto et al. 2018) and in the blood brain barrier (Okamoto and Yamanaka 2020). Once in the cytoplasm, Ecd is activated by the CYP450 enzyme called Shade, which converts it into its active form, the 20-hydroxyEcdysone (20E) (Petryk et al. 2003). Then, 20E binds to Ecd receptor (EcR), forming a dimer with the nuclear receptor Ultraspiracle, and the complex translocates into the nucleus, bind DNA specific sequence, called Ecd Responsive Element, which transcriptionally regulates Ecd target genes. However, circulating Ecd may impact larval organs in different ways depending on the instar, its concentration and the sensitivity of the targeted tissue, that also relates to potential differential capacities in its transport, activation and signalling. How these cellular mechanisms converge to tissue-restricted and/or systemic effects are not yet completely understood.

While studying the intestinal molecular responses involving microbe-mediated *Drosophila* adaptive growth, we identified Ecd signaling as an interesting *Lactobacilli*-mediated transcriptomic signature. Through functional and morphometrical analysis we reveal that, upon malnutrition, Ecd signaling is enhanced by the microbiota in larval enterocytes to adapt the midgut growth upon nutritional challenges.

Results and discussion

Larval midgut transcriptomic analysis reveals Ecdysone signature upon *Lp* association.

In order to identify the transcriptional networks contributing to adaptive growth in a context of malnutrition, a RNAseq experiment was performed on midguts of GF and *Lp*-associated animals to compare similar systemic contexts (*i.e.* size-matched animals) at two different developmental stages (Fig. 1A, Fig. S1A-B).

The analysis of the 2633 deregulated genes in both sizes led to the identification of 91 clusters using Functional Cluster Chart tool (DAVID genome), through which 53 showed an enrichment score (ES) >1,3 (Fig. 1B). Strikingly, the highest ES was obtained for a cluster named Ecdysteroid kinase-like (Fig. S1C) followed by families of mitochondrial proteins, proteases, signaling molecules. The early and late L3 regulated genes were then analyzed by Biological Process Direct (Fig. 1C). Some of the GOs were already identified in previous studies such as Immunity, Metabolism, Lipid Metabolism … (Erkosar et al. 2014; Storelli et al. 2011) but the "Response to Ecdysone" GO was newly highlighted in both larval sizes. Consistently, several Ecd related genes were identified as regulated upon *Lp*-association (Fig. S1D). Surpringsinly, while *Lp* association promotes larval systemic growth, no canonical effectors involved in tissue growth (such as Dilps, Hippo, dmyc or EGFR) were regulated in the intestine (Fig. S1E).

Further volcano plot analysis (Fig. 1D) show that for the early L3, 1624 regulated genes were identified, 876 genes were upregulated with 112 showing a FC > 2 and 747 genes were downregulated with 94 of them with FC > 2. For the late L3, 1462 genes were identified, 828 genes were upregulated with 173 showing a FC > 2 and 634 genes were downregulated with 75 of them with FC > 2. At both sizes, a cluster of genes was highly upregulated while none was shown downregulated. As expected, target genes related to IMD pathway activation such as *PGRP-SC2*, *PGRP-SC1* and *Pirk* as well as signatures of microbe-mediated intestinal maturation like *jon66cii* and *jon44E* were upregulated at both sizes upon *Lp* association (Fig. S2A, B).

This functional genomic analysis of the midgut from size-matched animals confirms the involvement of signals already identified using whole larvae RNAseq, such as the IMD pathway activation and carbohydrate/lipid-increased metabolisms. However, a novel noteworthy finding is the putative involvement of Ecd signaling on the microbiota-mediated intestinal response in a context of adaptive growth, which warrants further investigation.

Intestinal Ecdysone signals are not required for systemic growth promoted by *Lp*.

Since *Lp* promotes systemic adaptive growth and triggers an Ecd transcriptomic signature in the midgut, we wondered whether intestinal Ecd signals are involved in this process. First, the levels of 20E were quantified in the midgut, the fat body and the haemolymph of size-matched GF and *Lp*-associated animals. The detected levels of 20E were higher in *Lp*-associated midgut and haemolymph compared to GF (Fig. 2A-C). Thus, in size-matched animals, *Lp*-association sustains increased levels of circulating and intestinal Ecd active forms.

Then, functional analyses were performed on larvae in which the expression of EcR or shade were reduced in enterocytes through the use of RNA interference system. To this aim, axenic *mex-GAL4* virgins were crossed with males carrying transgenes encoding *EcR* or *shade* hairpins under the control of an Upstream Activating Sequence (UAS) to trigger enterocytes-specific RNA interference in progenies (Fig. S2C, D). A *Lp*-mediated support to adaptive growth was observed in control and knockdown animals compared to GF (Fig. 2D-G). EcR^{RNAi} GF pupae emerged later than their related control (Fig. 2E) while no supplemental delay was observed for $shade^{RNAi}$ GF animals upon knockdown (Fig. 2G). This phenomenon could be explained by genetic background and/or by additional deleterious effect of germ-freeness, as well as a putative contribution of EcR to intestinal functions that are important for systemic growth independently of the contributions of microbiota to adaptive growth.

Thus, there is no effect of reducing intestinal Ecd signaling on *Lp*-mediated adaptive growth. Nevertheless, the increased circulating levels of 20E in *Lp*-associated animals might account for their observed earlier maturation, consistently with previous data showing that Ecd target genes were upregulated in *Lp*-associated larvae (Storelli et al. 2011). Interestingly, beyond circulating levels, intestinal levels of 20E are higher in *Lp*-associated animals, raising the question of a putative impact of Ecd signaling in this tissue.

Intestinal Ecdysone signaling is required for the midgut growth effect mediated by *Lp*.

To further investigate the intestinal effect of Ecd, larval body length, gut length and gut/carcass ratio upon knockdown of main Ecd signaling effectors were evaluated. Size-matched *Lp*-associated larvae, $control^{RNAi}$ or EcR^{RNAi}, show longer midguts than their relative GF condition (Fig. 3A, B). Interestingly, intestinal EcR^{RNAi} leads to shortened guts compared to $control^{RNAi}$ *Lp*-associated animals. This strongly suggests that *EcR* is involved in the intestinal growth phenotype mediated by *Lp*. The gut/carcass ratios confirm that *Lp*-promoted midgut growth requires EcR in enterocytes (Fig. 3C). These results were further verified by knocking-down intestinal *shade* expression (Fig. 3D-F). Indeed, *shade* expression was previously detected by *in situ* hybridization in larval midguts (Chung et al. 2009). Moreover, the modENCODE data (Brown et al. 2014) and manually curated data (Flybase) show that *shade* is highly expressed in the L3 midgut. These results support the hypothesis that Ecd signaling is enhanced in enterocytes by the presence of *Lp* and allows for promoted gut growth.

Then, we tested whether a food supplementation with 20E was sufficient to further promote the midgut growth in absence of *Lp*, in a malnutrition context. While the systemic growth of animals is not affected by addition of 20E, a slight trend to faster midgut maturation of GF larvae is observed through the measurements of longer guts (Fig. S3). Thus, the intestinal Ecd signaling is required for the midgut growth effect mediated by *Lp* in a context of malnutrition. Considering the coordination of organ growth during development, we next wondered whether this tissue growth effect was specific to the midgut or could be detected in other organs.

Drosophila larval midgut is the unique organ benefiting an Ecd-mediated growth effect

To follow the developmental impact of *Lp* and Ecd signaling on different organs, axenic flies were placed on chronic malnutrition (Fig. 4A). Since larval tissue growth occurs through cell proliferation or endoreplication, the growths of two diploid and two polyploid organs were measured over time, Central Nervous System (CNS) and wing discs; and salivary glands and midgut respectively. While CNS, wing disc and salivary glands growths (Fig. 4 B-D) do not differ between absence or presence of bacteria, a clear difference is observed from midguts which show an increased length upon *Lp*-association around +16% (Fig. 4E-F).

Then, we wondered whether the whole intestine grows homogenously since *Lp* mostly accumulates in its first half (Storelli et al. 2018). For size-matched larvae, the *Lp*-associated animals show a longer gut than the GF, consistently with Fig. 4E (Fig. 4F-I), with a mean of 2.44 mm, 1.169 mm and 6.861 mm while the GF larvae show 1.855 mm, 1.234 mm and 4.120 mm, for anterior, middle and posterior parts respectively (Fig. 4J-L). Both anterior and posterior parts tend to be longer in *Lp*-associated larvae but the difference is only statistically significant for the posterior part. Thus, the promoted midgut growth is not homogenous and the posterior part mainly participates to the additional growth effect upon *Lp* association. In the anterior part, the cells and nuclei are bigger in *Lp*-associated than GF animals (Fig. 4M-N). For the posterior part, the cell area was significantly increased in *Lp* monoassociated animals compared to GF cell while no change was shown for the nucleus area (Fig. 4O-P). These results highlight that *Lp*-mediated midgut growth is at least sustained by increased cell growth. The difference in nuclei area (proportionally to the cell growth or not, depending on the gut part) suggests that the cellular mechanisms sustaining growth could be midgut-part specific. Thus, it seems that both anterior and posterior midgut parts participate to *Lp*-mediated local growth effect. This result was not expected since most of *Lp* resides in the first intestinal half part (Storelli et al. 2018). As recently reported for adult midgut (Blackie et al. 2024) it will be interesting to explore the 3D vicinity between anterior and posterior midgut growing compartments when they are folded in the larval "milieu interieur". Also, it will be interesting to test, beyond their shared growth phenotype, whether they respond differently at the mechanistical level to the presence of bacteria in the anterior compartment.

Taken together our results confirm the tight coordination of organ growth with systemic growth in the context of malnutrition. Indeed, upon dietary challenge, we highlight that only the midgut benefits an enhanced cellular growth from *Lp*-association. Thus, this finely tuned intestine plasticity supports the notion that members of the microbiota contribute to cellular mechanisms buffering the impact of environmental fluctuations (here, dietary) on organ growth.

To conclude, our midgut transcriptomic analysis led to the identification of known genes and pathways related to the presence of commensal *Lp* bacteria but also highlighted a new signature evoking Ecd signaling. Specifically, intestinal Ecd signaling is not rate-limiting for *Lp*-mediated adaptive growth. However, our results emphasize that Ecd conversion to 20E and Ecd signaling in enterocytes are promoted by *Lp*, an important member of *Drosophila* microbiota which supports intestinal midgut growth and maturation, in the context of malnutrition. This work establishes an unexpected role of Ecd signaling in larval midgut development and maturation in response to intestinal microbes and upon nutritional challenges. Our work paves the way to deciphering the signals delivered by the bacteria that are sensed at the host cellular level and to understand how this microbe-mediated Ecd-dependent midgut growth contributes to the *Drosophila* larval growth upon malnutrition at the host cellular level and to understand how this microbe-mediated Ecd-dependent midgut growth contributes to the *Drosophila* larval growth upon malnutrition.

Material and methods

Fly stocks and media

Drosophila conventional stocks were raised and maintained at 25°C with a 12/12 hours dark/light cycles on a yeast/cornmeal rich medium at 8.2g.L^{-1} agar (#20768.361, VWR), 80g.L^{-1} cornmeal flour (Westhove, Farigel maize H1), 80g.L^{-1} inactivated yeast (#24979.413, VWR), 5.2g.L^{-1} Methyl 4-hydroxybenzoate sodium salt (#106756, Merck) and 4mL.L^{-1} of 99% propionic acid (#409553, Carlo Elba). The axenic stocks were generated as described extensively in Ma et al. 2015, by bleaching embryos from conventional stocks and raising them on autoclaved rich medium supplemented with a cocktail of four antibiotics (Amp/Kan/Tetrac/Ery).

Nutritional challenge was performed using freshly prepared food in which the amount of inactivated yeast was reduced to 7g.L^{-1}. *Drosophila y,w* flies (from Bruno Lemaitre) were used as the reference strain. The following fly stocks were used: *y,w,mex-GAL4* (gift from Irene Miguel-Aliaga), *UAS-EcR*^{RNAi} (BDSC 9327)*,* *UAS-dsmCherry*^{RNAI} (BDSC 35785), *UAS-shade*^{RNAi} (VDRC 108911), and respective RNAi control lines (KK60101). All experimental crosses were performed using GF stocks at 29°C on depleted fresh food.

Bacterial culture and mono-association

Lactiplantibacillus plantarum^{WJL} (*Lp*) is a bacterial strain isolated from adult *Drosophila* midgut (Ryu et al., 2008). *Lp* was cultured in Man, Rogosa and Sharpe (MRS) broth medium overnight at 37°C without shaking as described in (Storelli et al. 2011). Briefly, *Lp* inoculation of tubes containing fly food is performed in order to obtain 10^8 CFUs.mL^{-1}. Inoculum is homogeneously spread on the surface once 40 embryos are deposited. For GF controls, an equal volume of sterile PBS is inoculated.

RNAseq analysis

GF or *Lp*-associated embryos from *y,w* axenic flies were raised on low-protein diet. Gut collection from 3rd instar size-matched (early^{L3} or late^{L3}) larvae for both experimental conditions was performed five and eight days after egg laying (AEL) for *Lp*-associated and eight and ten days AEL for GF animals. Five biological replicates of 15 guts/replicate for early^{L3} animals and 10 guts/replicate for Late^{L3} larva were obtained for the four different conditions. Guts were collected in RNA later (Ambion 1405055) in cryotubes (16466-064, VWR), which were directly frozen in liquid nitrogen. Then, samples were homogenized using the Precellys 24 tissue homogenizer (*03119-200-RD000* Bertin technologies*;* 2 x 6300rpm; 40s) with autoclaved 0.75mm glass beads (A554.1, Roth). RNA extraction was performed using the NucleoSpin kit (740955.250 Macherey Nagel) following the instructions and RNAs were quantified using Nanodrop (ND-2000, Thermofisher).

For RNA sequencing, samples were treated by the IGFL sequencing platform. Purification, quantification and quality check were performed using Dosage Qubit 2.0 – kit BR RNA (Thermofisher) and ARN Tapestation 2200 (Agilent). Libraries were generated following the online protocol of SENSE mRNA-Seq Library Prep Kit V2 for Illumina (https://www.hexabiogen.com) (Product: K01.24 – Lot: 7346) and quantified using Analyse Tapesation – D1000 ScreenTape®Dosage (Agilent). Raw data were treated by Pauline Joncour, a Bio-IT, to generate excel sheets.

Then, data were analyzed using the online software DAVID (DAVID Bioinformatics Resources, Laboratory of Human Retrovirology and Immunoinformatics (LHRI), USA) Functional Annotation Bioinformatics Microarray Analysis (https://david.ncifcrf.gov/). The whole analysis of the regulated genes in both sizes groups 2633 annotated genes that were organized into a functional annotation chart. These genes were grouped clusters, 53 out of the 91 clusters showed an enrichment score (ES) >1,3 (*i.e. p* value <0.05). The ES is defined as –log₁₀ (p_{adj}), mean of the p value of each term present in the cluster. Then, the genes from the two sizes were split in early ^{L3} and late ^{L3} and analyzed by Biological Process Direct with a $p_{adj} < 5.1\ 10^{-2}$ and presented as pie charts. Finally, volcano plots were generated using GraphPad Prism 8.

RT-qPCR

Total RNAs from five biological replicates (10 guts or mentioned in the legend if different) collected from size-matched larva were collected at different time point during development and were homogenized using the Precellys 24 tissue homogenizer with autoclaved 0,75/1mm glass beads.

This solution was treated for RNA purification using the NucleoSpin kit (Macherey- Nagel) following the instructions. Reverse transcription of 1µg of RNA was performed using the SuperScript II enzyme (Invitrogen) using random hexamers (Promega). Quantitative PCR was performed on an iQ5 Real- time PCR Detection System (Biorad) using the SYBR GreenER qPCR SuperMix (Invitrogen), 12ng of cDNA and the primer sets with the following sequences : *tubulin F 5’- TGTCGCGTGTGAAACACTTC-3’, R-5’- AGCAGGCGTTTCCAATCTG-3’ ; Rpl32 F 5’-ATGCTAAGCTGTCGCACAAATGR-3’, 5’-GTTCGATCCGTAACCGATGT-3’ ; jon66cii F 5’-AAACTGACCCCGGTCCAC-3’ , R 5’-CCTCCTCAGCCGGATAGC-3’ ; EcR F 5’-GCAAGGGGTTCTTTCGACG-3’, R 5’-CGGCCAGGACTTTTTCAG-3’ ; jon44E F 5’-ACAGCGCTAACCATGTGCT-3’, R 5’-GGTGTACTGGGCCTCGTG-3’ ; shade F 5’-CCCACCAAAACGTACAGGGA-3’, R 5’GTAATCCAGCAGCCTCGTCA-3’.* Melting curves of amplicons obtained were analyzed to ensure specific and unique amplification. PCR efficiency was calculated using serial dilution of cDNA. The ΔCt method was used for data analysis, using *Rpl32* and *tubulin* as reference genes. Results were expressed as relative $\Delta Ct^{gene}/\Delta Ct^{Rpl32-tubulin}$ ratios.

Larval size measurements and developmental timing determination

According to the bacterial culture and mono-association protocol, axenic eggs were inoculated with *Lp*, or with sterile PBS for controls, and incubated at 25°C or 29°C. The gut/carcass ratio was measured by assigning each gut to its initial body length, which allows for eliminating putative variability and thus highlights larvae unique features from a population. For developmental timing, pupae emergence was scored every day until all pupae have emerged. D50 was determined using D50App from (Matos et al. 2017) which is a Shiny app that calculates for the pupae emerged during a developmental experiment, the day when fifty percent of the pupae emerged.

Measurement of 20E titers

For guts, *yw* 3rd instar female larvae were dissected in ice-cooled PBS. A total of 10 guts by replicate (total 6) or 5 fat bodies (5 replicates) were pooled in 200µL of MetOH on ice. Samples were ground with a pestle and vortexed. After adding 300µL of MetOH, samples were centrifuged for 10min, 13000g at 4˚C. The supernatant was kept in a new tube and the pellet was re-extracted with 500µL MetOH, vortexed and centrifuged. Finally, the last extraction was performed using 500µL EtOH. The three collected supernatants were pooled and stored at -20˚C. For normalization, a duplicate of this experiment was performed and samples were quantify using the BCA method (SIGMA).

For haemolymph, *yw* 3rd instar female larvae were dried on tissue paper and placed on parafilm. The cuticle was gently pricked to collect 2µL from 8 larvae that were placed in 200µL of MetOH on ice (6 replicates). Then, the samples were treated the same way than described above. Evaporation of the samples was done using a SpeedVac and then dissolved in EIA buffer from the kit (A05120, Bertin) and treated following the manufacturer instructions.

Feeding experiments with 20E

Fly food medium was freshly cooked with 20 µg/mL of 20-hydroxyEcdysone (H5142, Sigma) or supplemented with a similar volume of EtOH. Then, the *yw* axenic embryos were deposited in the tubes as described previously (40 embryos/tube) and submitted to developmental timing and gut/carcass experiments.

Organ morphometrical analysis

Embryos from axenic flies were raised GF or *Lp* monoassociated at 25˚C on depleted diet until they reached the 3rd instar. Larvae were then collected during a period covering the 3rd instar (from 5 to 8 days after egg laying (D5 to D8) for *Lp*-associated larvae, n = 66, and D11 to D14 for GF animals, n=64)). Dissections were performed in a developmental window covering middle to end of L3 but rejecting wandering animals. For this developmental experiment, larval organs were dissected from different batches of *yw* flies GF or *Lp*-associated in ice-cooled Ca^{2+} free HL-3 solution (Stewart et al. 1994) (Budnik, Gorczyca, and Prokop 2006) on a Sylgard (sylgard® 184 silicone elastomer kit) coated Petri plate. From each larva, four organs (two diploid tissues (CNS and wing discs) and two polyploid tissues (midgut and salivary glands)) were then directly gently oriented on a poly-Lysine coated slide (without fixative agent) and imaged the stereomicroscope (M205FA, Leica). The carcass length (*i.e.* body length) was measured after dissection according to the distance between anterior and posterior pins and was plotted against organ area or length for each individual larva. Data are shown according the scaling relationship between two morphological traits developed by Julian Huxley demonstrating that an organismal shape as an equation $y = bx^{\alpha}$, x : size (length or mass) of the body and y : size of some trait and the log-log plots of the size of different traits among individuals of the same species often reveal linear scaling relationship with an intercept of b and a slope of α (Huxley 1924).

Gut parts morphometrical analysis

Embryos from axenic flies were raised GF or *Lp*-associated at 25˚C on low-protein diet until they reached the 3rd instar. Questioning the gut growth homogeneity, organs were dissected and fixed for 1 min in Bouin (HT10132, Sigma) and kept attached to the corresponding larval carcass (a read out for measuring body length) and imaged with a stereomicroscope M205FA (Leica). *Drosophila* larval midgut is a tube-like structure presenting heterogeneous transparency to transmitted light and which diameter fluctuates through its length (Shanbhag and Tripathi 2009). Taking advantage of these properties, the midgut was divided in three parts and their lengths were measured when GF and *Lp* monoassociated animals were raised on low nutrition diet. They were defined as anterior part that stops before acidic zone, middle part that comprises copper and iron cells regions, and the leftover zone was called posterior part and stops just before the Malpighian tubules.

For cell area and nucleus area, the 3rd instar larvae were dissected in ice-cooled Ca^{2+}-free HL-3 solution with a modified protocol from (Stewart et al. 1994) (Budnik, Gorczyca, and Prokop 2006). The guts were fixed in Bouin fixative for 2 min and washed in PBS 0.5% Triton X-100. After saturation with Normal goat serum (G9023, Sigma), mouse anti-Dlg were incubated at 1:1000 (4F3, DSHB) overnight at 4˚C. Hoechst 33342 was used at 0,5µg/mL (14533, Sigma). After washes, Alexa Fluor 555 anti-mouse conjugated secondary antibodies (Molecular Probes) were added at 1:200 for 2 h at room temperature. After washes, samples were mounted in Vectashield (H-1400 or H-1500 Vector Laboratories) and images were acquired as mosaics with the DM6000 (Leica) and analyzed with Fiji (NIH)**.**

Statistical analysis

Data representation and analysis was performed using Graphpad PRISM 8 software (www.graphpad.com). A total of 3 to 5 biological replicates were used for all experiments in order to ensure representativity and statistical significance. All samples were included in the analysis. Numbers of samples analyzed are indicated inside the bars. Statistical analyses were performed using different statistical tests that are mentioned in the figure legends. Error bars in all graphs indicate standard deviation ± SEM ;****$p < 0.001$; ***$p < 0.005$; ** $p < 0.01$; *$p < 0.05$ or ns.

Graphics

Schemes were created with Biorender.

Figures legends

Fig. 1: *Drosophila* larval midgut transcriptome reveals Ecd related signature.
(A) Experimental roadmap of midgut preparation and collection from size-matched *Lp*-associated and GF larvae at two different sizes named Early ^{L3} and Late ^{L3}. (B) According to RNAseq results, 2633 annotated genes were differentially regulated in both sizes. A total of 53 clusters of genes, out of 91, is presented with an enrichment score (ES) >1.3 (= *p* value < 0.05). (C) Biological Processes (BP Direct, $p_{adj} > 5.1\ 10^{-2}$) analysis of genes regulated is shown in pie charts for Size 1- Early^{L3} and Size 2 - Late^{L3}. The BPs are highlighted in boxes entitled with a general process name, in normal font BPs only found in Size 1, in **bold** BPs only found in Size 2 and in **bold** BPs common to sizes 1 and 2. (D) Volcano plots showing regulation of genes expression in Early^{L3} and Late^{L3}. All the genes are represented in the left panel while the right one focuses on those with $10 < -\log_{10}(p_{adj}) < 50$.

Fig. 2: Intestinal Ecd signals are not rate limiting for the *Lp*-mediated systemic growth
(A-C) Quantification of 20E in the haemolymph (A), the midgut (B) and the fat body (C) of size-matched GF and *Lp*-associated animals. Circulating levels of 20E are higher in *Lp*-associated animals (A) and amount of 20E is also increased in midguts compare to the GF (B). Note the general trend towards elevation in *Lp*-associated fat-bodies (C).
The DT (left panels: D, F) and their related D50 (right panels: E, G) are shown upon intestinal knockdown using *mex-GAL4* of *UAS-EcR*^{RNAi} (D-E) and *UAS-shade*^{RNAi} (F-G). For DT, controls crosses are shown in black filled (+*Lp)* or empty (GF) circles and knockdown conditions follow the same rule. For the D50 panels, each dot represents one biological replicate, color filled +*Lp*, gray filled when GF and in the box the median is shown with the min to max, dotted box for *Lp* and empty box for GF. Kruskal-Wallis test was performed; *p* values are indicated on the graph. These graphs are representative of at least 2 independent experiments with at least 4 biological replicates.

Fig. 3: Intestinal Ecd signaling is required for the local midgut growth effect mediated by *Lp*.
The carcass length (left panels, A, D), the gut length (middle panels, B, E) and the ratio gut/carcass (right panels, C, F) are shown upon the intestinal knockdown using *mex-GAL4* with *UAS-EcR*^{RNAi} (blue) and *UAS-shade*^{RNAi} (dark pink). Control crosses are shown in black filled (+*Lp)* or empty (GF) circles and knockdown conditions follow the same rule. Each dot represents one animal. In the box, the median is red with the 10 - 90 % quartile dotted line, box dotted for *Lp* and empty box for GF. ANOVA test was performed; *p* values are indicated on the graph.

Fig. 4: *Drosophila* larval midgut is the unique organ benefiting an Ecd-mediated growth effect
(A) Experimental roadmap for organ collection of L3 *yw* (D5 to D8 for *Lp* and D10 to D14 for GF); n = number of dissected larvae. (B-E) Organ measurements in diploid tissues (B) CNS and (C) imaginal wing discs, and polyploid tissues (D) salivary glands and (E) midguts. Each dot is an organ, in pink for *Lp* and black for GF. Simple linear regressions for each experimental group are shown in the graphs with p_s (*p* value slope) and p_e (*p* value elevation).
(F) Representative images of dissected guts attached to their carcass (read out for body length, green line) at D6 for *Lp* and D9 for GF animals. The anterior, middle and posterior parts are visualized in red, orange and yellow lines respectively. For size-matched animals (G), the gut is longer for *Lp*-associated larvae (H) as confirmed by the ratio gut/carcass (I). The length

measurements of anterior (J), middle (K) and posterior (L) regions highlight longer anterior and posterior parts. Midgut measurements of anterior part cell (M) and nucleus (N) areas and posterior part cell (O) and nucleus (P) areas. Measurements from *Lp*-associated larvae are shown in pink and GF larvae are in black (n= 6 guts, 105 cells and nuclei), in violin plots. For statistics unpaired t test was performed.

Bibiography

Blackie, Laura, Pedro Gaspar, Salem Mosleh, Oleh Lushchak, Lingjin Kong, Yuhong Jin, Agata P. Zielinska, et al. 2024. “The Sex of Organ Geometry.” *Nature* 630 (8016): 392–400. https://doi.org/10.1038/s41586-024-07463-4.

Boulan, Laura, Marco Milán, and Pierre Léopold. 2015. “The Systemic Control of Growth.” *Cold Spring Harbor Perspectives in Biology* 7 (12): a019117. https://doi.org/10.1101/cshperspect.a019117.

Brown, James B., Nathan Boley, Robert Eisman, Gemma E. May, Marcus H. Stoiber, Michael O. Duff, Ben W. Booth, et al. 2014. “Diversity and Dynamics of the Drosophila Transcriptome.” *Nature* 512 (7515): 393–99. https://doi.org/10.1038/nature12962.

Budnik, Vivian, Michael Gorczyca, and Andreas Prokop. 2006. “Selected Methods for the Anatomical Study of Drosophila Embryonic and Larval Neuromuscular Junctions.” *International Review of Neurobiology* 75:323–65. https://doi.org/10.1016/S0074-7742(06)75015-2.

Chung, Henry, Tamar Sztal, Shivani Pasricha, Mohan Sridhar, Philip Batterham, and Phillip J. Daborn. 2009. “Characterization of Drosophila Melanogaster Cytochrome P450 Genes.” *Proceedings of the National Academy of Sciences of the United States of America* 106 (14): 5731–36. https://doi.org/10.1073/pnas.0812141106.

Colombani, Julien, Sophie Raisin, Sophie Pantalacci, Thomas Radimerski, Jacques Montagne, and Pierre Léopold. 2003. “A Nutrient Sensor Mechanism Controls Drosophila Growth.” *Cell* 114 (6): 739–49. https://doi.org/10.1016/s0092-8674(03)00713-x.

Erkosar, Berra, Berra Erkosar Combe, Arnaud Defaye, Noémie Bozonnet, Denis Puthier, Julien Royet, and François Leulier. 2014. “Drosophila Microbiota Modulates Host Metabolic Gene Expression via IMD/NF-κB Signaling.” *PloS One* 9 (4): e94729. https://doi.org/10.1371/journal.pone.0094729.

Erkosar, Berra, Gilles Storelli, Mélanie Mitchell, Loan Bozonnet, Noémie Bozonnet, and François Leulier. 2015. “Pathogen Virulence Impedes Mutualist-Mediated Enhancement of Host Juvenile Growth via Inhibition of Protein Digestion.” *Cell Host & Microbe* 18 (4): 445–55. https://doi.org/10.1016/j.chom.2015.09.001.

Géminard, Charles, Eric J. Rulifson, and Pierre Léopold. 2009. “Remote Control of Insulin Secretion by Fat Cells in Drosophila.” *Cell Metabolism* 10 (3): 199–207. https://doi.org/10.1016/j.cmet.2009.08.002.

Huxley, Julian S. 1924. “Constant Differential Growth-Ratios and Their Significance.” *Nature* 114 (2877): 895–96. https://doi.org/10.1038/114895a0.

Ma, Dali, Gilles Storelli, Mélanie Mitchell, and François Leulier. 2015. “Studying Host-Microbiota Mutualism in Drosophila: Harnessing the Power of Gnotobiotic Flies.” *Biomedical Journal* 38 (4): 285–93. https://doi.org/10.4103/2319-4170.158620.

Matos, Renata C., Martin Schwarzer, Hugo Gervais, Pascal Courtin, Pauline Joncour, Benjamin Gillet, Dali Ma, et al. 2017. “D-Alanylation of Teichoic Acids Contributes to Lactobacillus Plantarum-Mediated Drosophila Growth during Chronic Undernutrition.” *Nature Microbiology* 2 (12): 1635–47. https://doi.org/10.1038/s41564-017-0038-x.

Okamoto, Naoki, Raghuvir Viswanatha, Riyan Bittar, Zhongchi Li, Sachiko Haga-Yamanaka, Norbert Perrimon, and Naoki Yamanaka. 2018. “A Membrane Transporter Is Required for Steroid Hormone Uptake in Drosophila.” *Developmental Cell* 47 (3): 294-305.e7. https://doi.org/10.1016/j.devcel.2018.09.012.

Okamoto, Naoki, and Naoki Yamanaka. 2020. “Steroid Hormone Entry into the Brain Requires a Membrane Transporter in Drosophila.” *Current Biology: CB* 30 (2): 359-366.e3. https://doi.org/10.1016/j.cub.2019.11.085.

Petryk, Anna, James T. Warren, Guillermo Marqués, Michael P. Jarcho, Lawrence I. Gilbert, Jonathan Kahler, Jean-Philippe Parvy, Yutai Li, Chantal Dauphin-Villemant, and Michael B. O'Connor. 2003. "Shade Is the Drosophila P450 Enzyme That Mediates the Hydroxylation of Ecdysone to the Steroid Insect Molting Hormone 20-Hydroxyecdysone." *Proceedings of the National Academy of Sciences of the United States of America* 100 (24): 13773–78. https://doi.org/10.1073/pnas.2336088100.

Schwarzer, Martin, Kassem Makki, Gilles Storelli, Irma Machuca-Gayet, Dagmar Srutkova, Petra Hermanova, Maria Elena Martino, et al. 2016. "Lactobacillus Plantarum Strain Maintains Growth of Infant Mice during Chronic Undernutrition." *Science (New York, N.Y.)* 351 (6275): 854–57. https://doi.org/10.1126/science.aad8588.

Shanbhag, Shubha, and Subrata Tripathi. 2009. "Epithelial Ultrastructure and Cellular Mechanisms of Acid and Base Transport in the Drosophila Midgut." *The Journal of Experimental Biology* 212 (Pt 11): 1731–44. https://doi.org/10.1242/jeb.029306.

Shingleton, Alexander W., Jayatri Das, Lucio Vinicius, and David L. Stern. 2005. "The Temporal Requirements for Insulin Signaling during Development in Drosophila." *PLoS Biology* 3 (9): e289. https://doi.org/10.1371/journal.pbio.0030289.

Stewart, B. A., H. L. Atwood, J. J. Renger, J. Wang, and C. F. Wu. 1994. "Improved Stability of Drosophila Larval Neuromuscular Preparations in Haemolymph-like Physiological Solutions." *Journal of Comparative Physiology. A, Sensory, Neural, and Behavioral Physiology* 175 (2): 179–91. https://doi.org/10.1007/BF00215114.

Storelli, Gilles, Arnaud Defaye, Berra Erkosar, Pascal Hols, Julien Royet, and François Leulier. 2011. "Lactobacillus Plantarum Promotes Drosophila Systemic Growth by Modulating Hormonal Signals through TOR-Dependent Nutrient Sensing." *Cell Metabolism* 14 (3): 403–14. https://doi.org/10.1016/j.cmet.2011.07.012.

Storelli, Gilles, Maura Strigini, Théodore Grenier, Loan Bozonnet, Martin Schwarzer, Catherine Daniel, Renata Matos, and François Leulier. 2018. "Drosophila Perpetuates Nutritional Mutualism by Promoting the Fitness of Its Intestinal Symbiont Lactobacillus Plantarum." *Cell Metabolism* 27 (2): 362-377.e8. https://doi.org/10.1016/j.cmet.2017.11.011.

Yamanaka, Naoki, Guillermo Marqués, and Michael B. O'Connor. 2015. "Vesicle-Mediated Steroid Hormone Secretion in Drosophila Melanogaster." *Cell* 163 (4): 907–19. https://doi.org/10.1016/j.cell.2015.10.022.

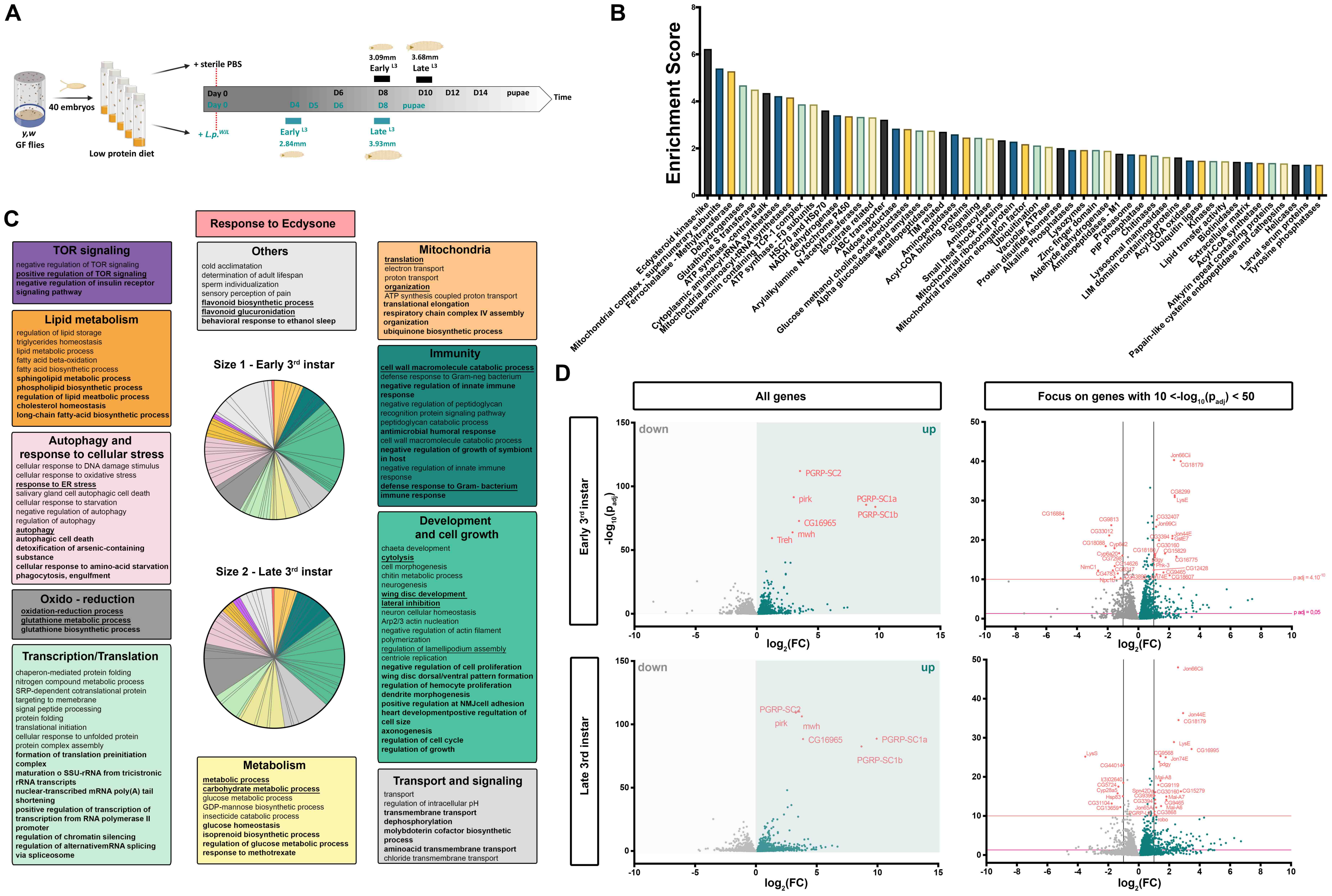

Response to Ecdysone

TOR signaling
negative regulation of TOR signaling
positive regulation of TOR signaling
negative regulation of insulin receptor signaling pathway

Lipid metabolism
regulation of lipid storage
triglycerides homeostasis
lipid metabolic process
fatty acid beta-oxidation
fatty acid biosynthetic process
sphingolipid metabolic process
phospholipid biosynthetic process
regulation of lipid meatbolic process
cholesterol homeostasis
long-chain fatty-acid biosynthetic process

Autophagy and response to cellular stress
cellular response to DNA damage stimulus
cellular response to oxidative stress
response to ER stress
salivary gland cell autophagic cell death
cellular response to starvation
negative regulation of autophagy
regulation of autophagy
autophagy
autophagic cell death
detoxification of arsenic-containing substance
cellular response to amino-acid starvation
phagocytosis, engulfment

Oxido - reduction
oxidation-reduction process
glutathione metabolic process
glutathione biosynthetic process

Transcription/Translation
chaperon-mediated protein folding
nitrogen compound metabolic process
SRP-dependent cotranslational protein targeting to memebrane
signal peptide processing
protein folding
translational initiation
cellular response to unfolded protein
protein complex assembly
formation of translation preinitiation complex
maturation o SSU-rRNA from tricistronic rRNA transcripts
nuclear-transcribed mRNA poly(A) tail shortening
positive regulation of transcription of transcription from RNA polymerase II promoter
regulation of chromatin silencing
regulation of alternativemRNA splicing via spliceosome

Others
cold acclimatation
determination of adult lifespan
sperm individualization
sensory perception of pain
flavonoid biosynthetic process
flavonoid glucuronidation
behavioral response to ethanol sleep

Metabolism
metabolic process
carbohydrate metabolic process
glucose metabolic process
GDP-mannose biosynthetic process
insecticide catabolic process
glucose homeostasis
isoprenoid biosynthetic process
regulation of glucose metabolic process
response to methotrexate

Mitochondria
translation
electron transport
proton transport
organization
ATP synthesis coupled proton transport
translational elongation
respiratory chain complex IV assembly organization
ubiquinone biosynthetic process

Immunity
cell wall macromolecule catabolic process
defense response to Gram-neg bacterium
negative regulation of innate immune response
negative regulation of peptidoglycan recognition protein signaling pathway
peptidoglycan catabolic process
antimicrobial humoral response
cell wall macromolecule catabolic process
negative regulation of growth of symbiont in host
negative regulation of innate immune response
defense response to Gram- bacterium
immune response

Development and cell growth
chaeta development
cytolysis
cell morphogenesis
chitin metabolic process
neurogenesis
wing disc development
lateral inhibition
neuron cellular homeostasis
Arp2/3 actin nucleation
negative regulation of actin filament polymerization
regulation of lamellipodium assembly
centriole replication
negative regulation of cell proliferation
wing disc dorsal/ventral pattern formation
regulation of hemocyte proliferation
dendrite morphogenesis
positive regulation at NMJcell adhesion
heart developmentpostive regultation of cell size
axonogenesis
regulation of cell cycle
regulation of growth

Transport and signaling
transport
regulation of intracellular pH
transmembrane transport
dephosphorylation
molybdoterin cofactor biosynthetic process
aminoacid transmembrane transport
chloride transmembrane transport

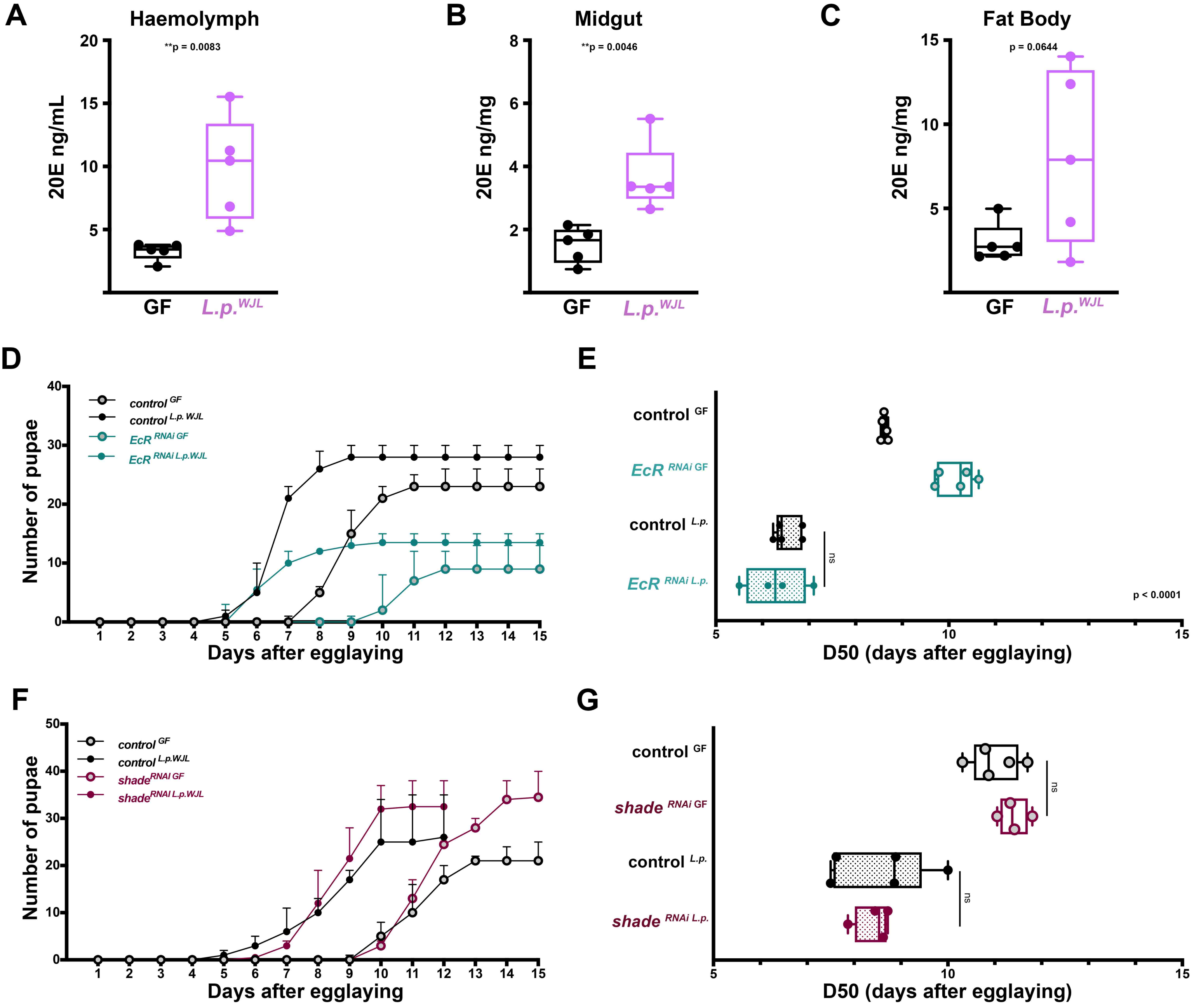
A
Haemolymph
**p = 0.0083
20E ng/mL
20
15
10
5
GF
L.p.WJL
B
Midgut
**p = 0.0046
20E ng/mg
8
6
4
2
GF
L.p.WJL
C
Fat Body
p = 0.0644
20E ng/mg
15
10
5
GF
L.p.WJL
D
Number of pupae
40
30
20
10
0
control GF
control L.p. WJL
EcR RNAi GF
EcR RNAi L.p.WJL
1 2 3 4 5 6 7 8 9 10 11 12 13 14 15
Days after egglaying
E
control GF
EcR RNAi GF
control L.p.
EcR RNAi L.p.
ns
p < 0.0001
5
10
15
D50 (days after egglaying)
F
Number of pupae
50
40
30
20
10
0
control GF
control L.p.WJL
shadeRNAi GF
shadeRNAi L.p.WJL
1 2 3 4 5 6 7 8 9 10 11 12 13 14 15
Days after egglaying
G
control GF
shade RNAi GF
control L.p.
shade RNAi L.p.
ns
ns
5
10
15
D50 (days after egglaying)

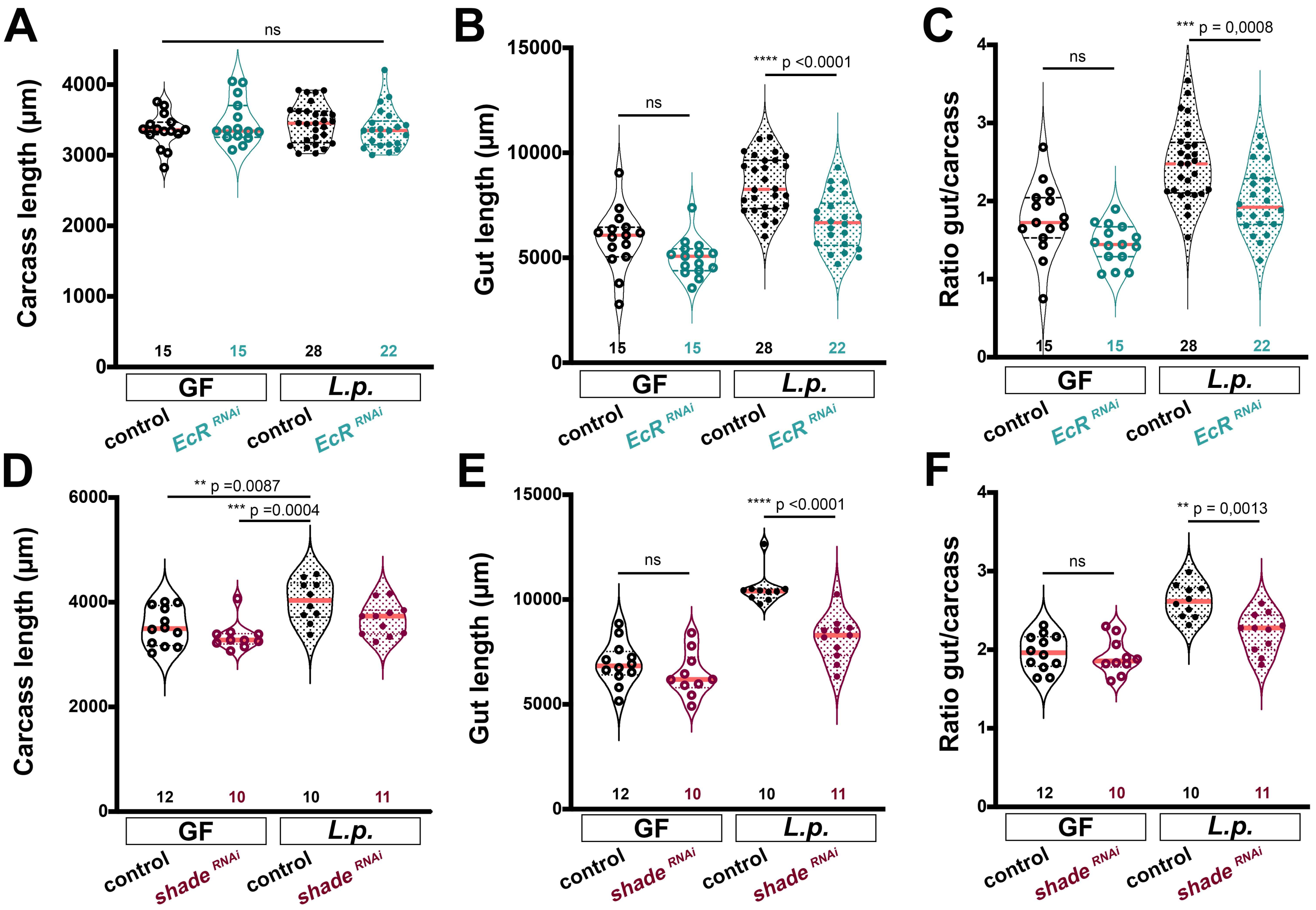
A
ns
Carcass length (µm)
4000
3000
2000
1000
0
15
15
28
22
GF
L.p.
control
EcR RNAi
control
EcR RNAi
B
**** p <0.0001
ns
Gut length (µm)
15000
10000
5000
0
15
15
28
22
GF
L.p.
control
EcR RNAi
control
EcR RNAi
C
*** p = 0,0008
ns
Ratio gut/carcass
4
3
2
1
0
15
15
28
22
GF
L.p.
control
EcR RNAi
control
EcR RNAi
D
** p =0.0087
*** p =0.0004
Carcass length (µm)
6000
4000
2000
0
12
10
10
11
GF
L.p.
control
shade RNAi
control
shade RNAi
E
**** p <0.0001
ns
Gut length (µm)
15000
10000
5000
0
12
10
10
11
GF
L.p.
control
shade RNAi
control
shade RNAi
F
** p = 0,0013
ns
Ratio gut/carcass
4
3
2
1
0
12
10
10
11
GF
L.p.
control
shade RNAi
control
shade RNAi

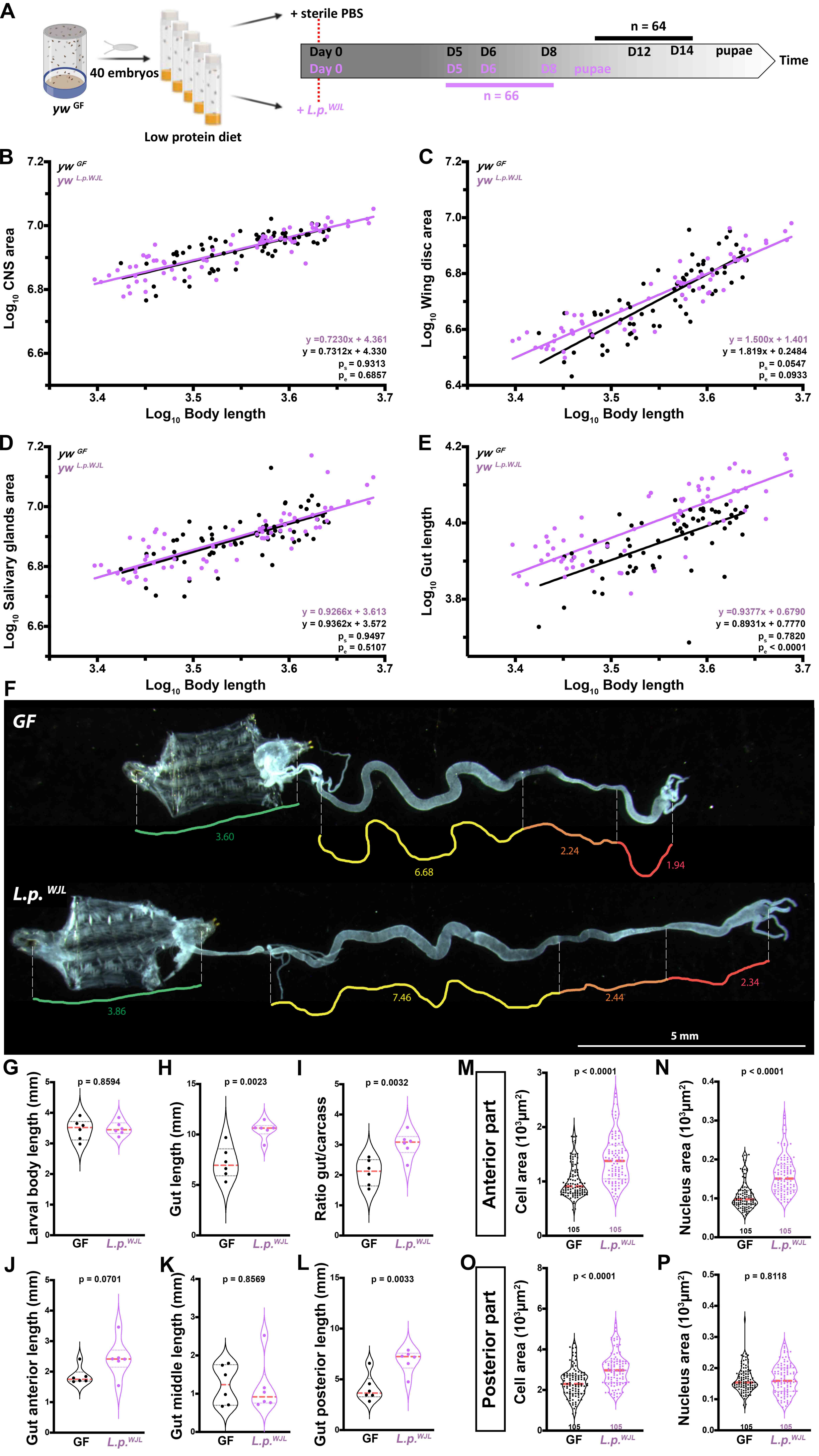
A
40 embryos
yw GF
Low protein diet
+ sterile PBS
+ L.p. WJL
n = 64
Day 0
D5
D6
D8
D12
D14
pupae
Time
Day 0
D5
D6
D8
pupae
n = 66
B
yw GF
yw L.p.WJL
Log10 CNS area
Log10 Body length
y =0.7230x + 4.361
y = 0.7312x + 4.330
ps = 0.9313
pe = 0.6857
C
Log10 Wing disc area
y = 1.500x + 1.401
y = 1.819x + 0.2484
ps = 0.0547
pe = 0.0933
D
Log10 Salivary glands area
y = 0.9266x + 3.613
y = 0.9362x + 3.572
ps = 0.9497
pe = 0.5107
E
Log10 Gut length
y =0.9377x + 0.6790
y = 0.8931x + 0.7770
ps = 0.7820
pe < 0.0001
F
GF
3.60
6.68
2.24
1.94
L.p. WJL
3.86
7.46
2.44
2.34
5 mm
G
Larval body length (mm)
p = 0.8594
H
Gut length (mm)
p = 0.0023
I
Ratio gut/carcass
p = 0.0032
M
Anterior part
Cell area (10³µm²)
p < 0.0001
N
Nucleus area (10³µm²)
p < 0.0001
J
Gut anterior length (mm)
p = 0.0701
K
Gut middle length (mm)
p = 0.8569
L
Gut posterior length (mm)
p = 0.0033
O
Posterior part
Cell area (10³µm²)
p < 0.0001
P
Nucleus area (10³µm²)
p = 0.8118
105
105
GF
L.p.WJL